

Issues and Observations on Applications of the Constrained-Path Monte Carlo Method to Many-Fermion Systems

J. Carlson, J.E. Gubernatis, and G. Ortiz

Theoretical Division, Los Alamos National Laboratory, Los Alamos, NM 87545

Shiwei Zhang

Departments of Physics and Applied Science

College of William and Mary, Williamsburg, VA 23187

(October 17, 2018)

Abstract

We report several important observations that underscore the distinctions between the constrained-path Monte Carlo method and the continuum and lattice versions of the fixed-node method. The main distinctions stem from the differences in the state space in which the random walk occurs and in the manner in which the random walkers are constrained. One consequence is that in the constrained-path method the so-called mixed estimator for the energy is not an upper bound to the exact energy, as previously claimed. Several ways of producing an energy upper bound are given, and relevant methodological aspects are illustrated with simple examples.

PACS numbers: 02.70.-c, 71.10.+x, 71.20.Ad, 71.45.Nt

I. INTRODUCTION

It is arguable that the fixed-node¹ and constrained-path² quantum Monte Carlo methods are the two most powerful and useful simulation techniques for computing accurate ground-state ($T = 0$ K) properties of large systems of interacting quantum particles. As the significantly older method, the fixed-node method has been well studied, and its properties are well documented.³ Less is known about the constrained-path method, but because of our recent use of this method,^{4–8} we now can report several important experiences and observations that underscore features distinguishing it from both the continuum^{9,10} and lattice¹¹ versions of the fixed-node method.

There is a very strong analogy between the fixed-node and constrained-path methods. Both, in a sense, are auxiliary-field methods, both project the ground-state wave function from a trial wave function by an importance-sampled, branched random walk, and both place a constraint on this random walk to prevent the fermion sign problem from rapidly producing exponentially growing variances. A number of technical details for their implementation are the same. In fact, the formal development of the constrained-path method² relied on the existence of the fixed-node method. The three principal differences between the methods are (a) the state space where random walks have their support, (b) the manner by which random walkers are constrained, and (c) the part of the imaginary-time propagator that is stochastically sampled.

The continuum version of the fixed-node method works in a first quantized representation and operates in coordinate space. The basis states are the complete orthonormal set of the particle configurations. The constrained-path method works in a second quantized representation and operates in Fock space. Its basis states are the over-complete non-orthonormal set of Slater determinants

$$|\phi\rangle = a_1^\dagger a_2^\dagger \cdots a_N^\dagger |0\rangle, \quad (1)$$

where the $a_i^\dagger = \sum_{j=1}^M \Phi_{ij} c_j^\dagger$ creates a fermion in a quasi particle state i defined relative to M possible single particle states j created by the operator c_j^\dagger , and $|0\rangle$ represents the vacuum.

(In the one-band Hubbard model M will be the number of lattice sites.) In this basis classes of many-electron wave functions like the BCS wave function are more easily used, and many-particle expectation values like superconducting pairing correlation functions are more easily evaluated than possible with the fixed-node method.² The ease in the evaluation of ground-state observables, for example, is a consequence of the ease in evaluating single-particle propagators and using Wick's theorem¹² to express any multi-particle propagator as a linear combination of products of one-particle propagators.

The differences in bases generate a difference in the way the random walks are constrained. Both methods rely on a trial state $|\Psi_T\rangle$ to perform the constraint. In the continuum version of the fixed-node method with \mathbf{r}_i representing a particle's position, the random walks are confined within a surface defined by $\langle \mathbf{R} | \Psi_T \rangle = \Psi_T(\mathbf{R}) \equiv \Psi_T(\mathbf{r}_1, \mathbf{r}_2, \dots, \mathbf{r}_N) > 0$, whereas in the constrained-path method, only random walkers $|\phi\rangle$ satisfying $\langle \Psi_T | \phi \rangle > 0$ are permitted. The fixed-node method solves Schrödinger's equation for the ground-state wave function inside the nodal surface. Unless that surface is exact, only an approximate solution is obtainable. The constrained-path condition, as we will discuss, has different implications. In certain cases, including some simple examples detailed below, the constraint is never invoked and hence the constrained-path method can sometimes produce the exact solution even for systems of interacting fermions. We also give examples where the solution, though approximate, is extremely accurate. These examples include a closed-shell Hubbard model with a large positive U .

The resulting stochastic dynamics in the basis space (both coordinate and Slater determinantal manifolds) is a Markov process generated by a conditional probability connected to the imaginary-time τ propagator $\exp[-\tau H]$, where $H = T + V$ is the Hamiltonian representing the system and, as usual, T and V are the kinetic and potential energy operators, respectively. The kinetic energy propagator is non-diagonal in the coordinate basis representation and its action can be viewed as a diffusion process in the basis space. On the other hand, in the Slater determinant representation it is the potential energy kernel which, after a Hubbard-Stratonovich transformation, generates the Markov chain. As a consequence,

non-interacting problems do not suffer from the fermion sign instability.

The main purpose of the paper is to illustrate that the constrained-path method **is not** equivalent to the fixed-node method in the space of Slater determinants. In Section II we will summarize the essential mathematical structure of both methods. In Section III, we discuss the mixed estimator for the energy and the extent to which it is an upper bound on the ground-state energy. In particular, we will conclude and illustrate that in the constrained-path method it is not, in general, an upper bound, contrary to previous claims and to the fixed-node method. In Section IV we provide a correction to the mixed estimator that makes it a rigorous upper bound, plus several alternative ways to produce energy estimates that are upper bounds. In Section V, we conclude by commenting on areas needing additional clarification and several other differences between the methods. Some of these differences will be illustrated in the Appendix where we present a constrained-path simulation on a small toy problem for which many of the details can be generated analytically. Of particular emphasis here will be the effects of matrix stabilization.

II. SUMMARY OF THE TWO METHODS

Both the fixed-node and constrained-path methods project the ground state $|\Psi_0\rangle$ from the long-time solution of the imaginary-time τ representation of Schrödinger's equation specified by a Hamiltonian H

$$\frac{\partial|\Psi\rangle}{\partial\tau} = -(H - E_0)|\Psi\rangle . \quad (2)$$

Provided $N_0 = \langle\Psi_0|\Psi(0)\rangle \neq 0$ and H is time-independent, the formal solution

$$|\Psi(\tau)\rangle = e^{-\tau(H-E_0)}|\Psi(0)\rangle \quad (3)$$

has the property

$$\lim_{\tau \rightarrow \infty} |\Psi(\tau)\rangle = N_0|\Psi_0\rangle . \quad (4)$$

On the computer this limit is accomplished iteratively

$$|\Psi'\rangle = e^{-\Delta\tau(H-E_T)}|\Psi\rangle, \quad (5)$$

where $\Delta\tau$ is a small number, $n\Delta\tau = \tau$, n is the current number of iterations (often called time slices), and E_T is a trial guess at the ground-state energy E_0 . The iterative process is converted into a stochastic sampling process. As the matrix elements of the propagator $\exp[-\tau(H - E_T)]$ between different anti-symmetric wave functions are not always positive definite, constraints in the sampling are necessary to insure this. Additionally, importance sampling is also required to control the variances of computed results. If E_T is adjusted so that it equals E_0 , then as $\tau \rightarrow \infty$, the iteration becomes stationary, i.e. $\partial|\Psi\rangle/\partial\tau = 0$ and $|\Psi\rangle \propto |\Psi_0\rangle$.

For simplicity, we will exclude branching from our discussions and consider only time-reversal symmetric Hamiltonians, that is, real symmetric operators for which the ground-state wave functions can always be chosen to be real. This analysis leaves out the very important case of systems in the presence of external magnetic fields.¹³ Here we compare the constrained-path method to the continuum fixed-node approach. There are some technical differences between the continuum fixed-node method^{9,10} and the lattice version¹¹ we prefer to omit. In this regard we comment that the constrained-path method does not distinguish between lattice and continuum fermions: both are treated on an equal footing.

A. Fixed-Node method

In the fixed-node method, one represents the ground state as $|\Psi_0\rangle = \sum_{\mathbf{R}} |\mathbf{R}\rangle \langle \mathbf{R} | \Psi_0 \rangle = \sum_{\mathbf{R}} \Psi_0(\mathbf{R}) |\mathbf{R}\rangle$ where $\Psi_0(\mathbf{R}) > 0$. Asymptotically, the Monte Carlo procedure samples from the distribution $P(\mathbf{R}) = \Psi_0(\mathbf{R}) / \sum_{\mathbf{R}} \Psi_0(\mathbf{R})$.

In the fixed-node method, one projects the iteration onto the basis of particle configurations $\{|\mathbf{R}\rangle\}$

$$|\Psi'\rangle = e^{-\Delta\tau(H-E_T)}|\Psi\rangle. \quad (6)$$

Projecting this equation onto $\langle \mathbf{R}' |$ and inserting $\sum_{\mathbf{R}} |\mathbf{R}\rangle \langle \mathbf{R}| = 1$ leads to

$$\langle \mathbf{R}' | \Psi' \rangle = \Psi'(\mathbf{R}') = \sum_{\mathbf{R}} \langle \mathbf{R}' | e^{-\Delta\tau(H-E_T)} | \mathbf{R} \rangle \Psi(\mathbf{R}) , \quad (7)$$

and correspondingly the imaginary-time Schrödinger's equation becomes

$$-\frac{\partial \Psi(\mathbf{R}, \tau)}{\partial \tau} = [-D\nabla^2 + V(\mathbf{R}) - E_T] \Psi(\mathbf{R}, \tau) \quad (8)$$

where $D = \hbar^2/2m$, m is the fermion mass, and $V(\mathbf{R})$ is the potential energy.

$\Psi(\mathbf{R})$ must be positive to be interpreted as the limiting probability distribution of the Markov chain. Fixing the node forces this by prohibiting any change in the particle configuration $\mathbf{R} \rightarrow \mathbf{R}'$ that changes the sign of $\Psi(\mathbf{R})$. We will denote the ground state produced under the constraint, i.e. under the fixed-node condition, as $|\Psi_c\rangle$ and the eigenvalue of the propagation (Eq. 6) as $\exp[-\Delta\tau(E_g - E_T)]$. This eigenvalue defines E_g , the growth energy.

After the so-called short-time approximation is made on the kernel of the integral, which is equivalent to making a Trotter approximation and a Hubbard-Stratonovich transformation on the exponential of the kinetic energy,² the positivity of $\langle \mathbf{R}' | \exp[-\Delta\tau(H - E_T)] | \mathbf{R} \rangle$ is trivially satisfied so it can be interpreted as a transition probability defining a Markov chain. We will call the resulting approximation $K(\mathbf{R} \rightarrow \mathbf{R}')$.

It is critical to importance sample in order to reduce statistical fluctuations, especially when the potential $V(\mathbf{R})$ has some singularities, for example, like the $1/r$ Coulomb singularity. This means we generate a new distribution $\tilde{\Psi}_c(\mathbf{R}) \equiv \Psi_T(\mathbf{R})\Psi_c(\mathbf{R})$ satisfying

$$\tilde{\Psi}'_c(\mathbf{R}') = \sum_{\mathbf{R}} \tilde{K}(\mathbf{R} \rightarrow \mathbf{R}') \tilde{\Psi}_c(\mathbf{R}) , \quad (9)$$

where $\tilde{K}(\mathbf{R} \rightarrow \mathbf{R}') = \Psi_T(\mathbf{R}')K(\mathbf{R} \rightarrow \mathbf{R}')/\Psi_T(\mathbf{R})$. The new configurations are now sampled with a different probability. The new distribution also satisfies a different equation of motion

$$-\frac{\partial \tilde{\Psi}_c(\mathbf{R}, \tau)}{\partial \tau} = -D\nabla^2 \tilde{\Psi}_c(\mathbf{R}, \tau) + D\nabla \cdot [\tilde{\Psi}_c(\mathbf{R}, \tau) \mathbf{F}(\mathbf{R})] + (E_L(\mathbf{R}) - E_T) \tilde{\Psi}_c(\mathbf{R}, \tau) , \quad (10)$$

where the “quantum drift” $\mathbf{F} = 2\nabla \ln \Psi_T$ and the “local energy” $E_L(\mathbf{R}) = H\Psi_T(\mathbf{R})/\Psi_T(\mathbf{R})$.

The Monte Carlo procedure represents the multi-dimensional integral as a set of random walkers $\{|\mathbf{R}\rangle\}$ where each member of the set is a different allowed particle configuration. A new configuration $|\mathbf{R}'\rangle$ is sampled from $\tilde{K}(\mathbf{R} \rightarrow \mathbf{R}')$ and rejected, thereby terminating this random walker, if the resulting value of the wave function is negative.

Since $\Psi_c(\mathbf{R}, \tau) = \tilde{\Psi}_c(\mathbf{R}, \tau)/\Psi_T(\mathbf{R})$, a variational upper bound to the true energy is

$$E_v = \frac{\sum_{\mathbf{R}} \Psi_c H \Psi_c}{\sum_{\mathbf{R}} \Psi_c^2} \geq E_0. \quad (11)$$

At large times walkers are distributed with a probability density $\Psi_T(R)\Psi_c(R)$, and both Ψ_T and Ψ_c go to zero linearly near the nodal surface. Since the Hamiltonian and the constraint are all local operators, this implies that the growth energy E_g is equal to the mixed estimate of the energy E_m ^{9,10}

$$E_g = E_m \equiv \frac{\langle \Psi_T | H | \Psi_c \rangle}{\langle \Psi_T | \Psi_c \rangle} = \frac{\sum_{\mathbf{R}} \Psi_c H \Psi_T}{\sum_{\mathbf{R}} \Psi_c \Psi_T} = \frac{\sum_{\mathbf{R}} \tilde{\Psi}_c(\mathbf{R}, \tau) E_L(\mathbf{R})}{\sum_{\mathbf{R}} \tilde{\Psi}_c(\mathbf{R}, \tau)}. \quad (12)$$

The constrained propagator is identical to the exact one except near the nodal surface where the constraint acts. The constraint discards contributions that are orthogonal to both Ψ_T and Ψ_c , and hence this region gives no net contribution to either $\langle \Psi_T | H | \Psi_c \rangle$ or $\langle \Psi_c | H | \Psi_c \rangle$. Therefore, the variational estimate of the energy E_v is identical to E_g and E_m , and all are variational upper bounds. E_m is more easily, accurately, and efficiently computed than E_g or E_v .

Several characteristics of the fixed-node method are: 1) The nodal surface of $\Psi_c(\mathbf{R})$ is exactly the same as that of $\Psi_T(\mathbf{R})$; 2) The exact ground-state energy is obtained *only if* the nodal surface of $\Psi_T(\mathbf{R})$ is exact; and 3) even for the trivial case of $V(\mathbf{R}) = 0$, unless the exact nodal surface is used, only an approximate solution is produced.

B. Constrained-Path Method

In the constrained-path method, one represents the ground state as $|\Psi_0\rangle = \sum_{\phi} c_{\phi} |\phi\rangle$ where the Slater determinants $|\phi\rangle$ are chosen so that all $c_{\phi} > 0$. Asymptotically, the Monte

Carlo procedure samples from the distribution $\pi(\phi) = c_\phi / \sum_\phi c_\phi$. The decomposition of $|\Psi_0\rangle$ in terms of the $|\phi\rangle$'s is not unique. One could just as well have $|\Psi_0\rangle = \sum_\phi d_\phi |\phi\rangle$ where $d_\phi > 0$. We will simply write $|\Psi_0\rangle = \sum_\phi |\phi\rangle$.

The constrained-path method works in a basis of Slater determinants. Again one iterates Eq. 6, placing constraints on the random walks. A different kind of constraint is needed because a different basis is used. Here the sign problem is caused by transitions from a region where the overlap $\langle \Psi_T | \phi \rangle$ is positive to a region where it is negative. These two regions are not physically distinguishable; they involve merely the exchange of fermions. Hence an arbitrary wave function can always be expanded in the restricted bases where $\langle \Psi_T | \phi \rangle$ is purely positive or purely negative. The original propagation mixes these two degenerate bases indiscriminately, causing a sign problem.

To break this plus-minus symmetry, the random walks are constrained to the region $\langle \Psi_T | \phi \rangle > 0$. This is an approximation because in general a wave function will have both positive and negative coefficients c_ϕ when expressed in this basis. However, the constrained propagation yields all the $c_\phi > 0$. To compare with the fixed-node method, we sketch some additional details: After the application of a Trotter approximation and Hubbard-Stratonovich transformation, the iterative equation becomes

$$|\Psi'\rangle = \sum_{\mathbf{x}} P(\mathbf{x}) B(\mathbf{x}) |\Psi\rangle, \quad (13)$$

where \mathbf{x} (the Hubbard-Stratonovich field) is to be interpreted as a multi-dimensional random variable distributed according to $P(\mathbf{x})$, and $B(\mathbf{x})$ is an operator approximating $\exp[-\Delta\tau H]$ for a given value of the random variable, whose general structure is a product of exponentials of one-body operators. $B(\mathbf{x})$ has the property of transforming one Slater determinant into another. The Monte Carlo method is used to evaluate the multi-dimensional integration by using multiple random walkers $|\phi\rangle$, and for each walker, sampling a \mathbf{x} from $P(\mathbf{x})$ and then generating a new walker

$$|\phi'\rangle = B(\mathbf{x}) |\phi\rangle. \quad (14)$$

Thus, if $\langle \Psi_T | \phi' \rangle > 0$, $\langle \Psi_T | B(\mathbf{x}) | \phi \rangle > 0$.

Since the basis of Slater determinants is non-orthogonal and over-complete, each member of the basis, in general, is a linear combination of the others, i.e., $|\phi\rangle = \sum_{\phi'} a_{\phi'} |\phi'\rangle$. A prime is on the summation symbol because while the summation may be over an infinite number of Slater determinants, the ones used need not exhaust the basis. While $|\Psi_T\rangle$ may constrain a $|\phi\rangle$ to be in the “positive” set, this $|\phi\rangle$ can overlap with a state in the “negative” set. In contrast to the fixed-node condition, the constrained-path condition does not separate the basis into orthogonal sets. Whereas the fixed-node condition must produce an approximate solution unless the nodes are exact, the constrained-path method can sometimes produce the exact solution even if the constraining wave function is approximate and has the wrong nodal surface in configuration space.

Importance sampling is also implemented in the constrained-path method. With $|\tilde{\phi}\rangle = \langle \Psi_T | \phi \rangle |\phi\rangle$ the iteration on each walker becomes

$$|\tilde{\phi}'\rangle = B(\mathbf{x}) |\tilde{\phi}\rangle, \quad (15)$$

but now the random variable \mathbf{x} is sampled from $\tilde{P}(\mathbf{x}) \propto \langle \Psi_T | \phi' \rangle P(\mathbf{x}) / \langle \Psi_T | \phi \rangle$. We have $|\tilde{\Psi}\rangle = \sum_{\phi} \langle \Psi_T | \phi \rangle |\phi\rangle$.

Again a variational estimate of the energy E_v can be constructed from $|\Psi_c\rangle$

$$E_v = \frac{\langle \Psi_c | H | \Psi_c \rangle}{\langle \Psi_c | \Psi_c \rangle} = E_g \geq E_0, \quad (16)$$

but now the connection among E_v , E_g and E_m is unclear because the constraint discards configurations which are orthogonal to $|\Psi_T\rangle$ and these discarded configurations are not necessarily orthogonal to $|\Psi_c\rangle$. As we will argue in the next section, the mixed estimator is not always an upper bound to E_0 . This retracts previous claims of E_m being an upper bound.²

Several characteristics of the constrained-path method are: 1) The nodal surface of $\langle \phi | \Psi_c \rangle$ is not the same as that of $\langle \phi | \Psi_T \rangle$; 2) In some cases, the exact ground-state energy can be obtained *even if* the nodal surface of $\langle \phi | \Psi_T \rangle$ is approximate; and 3) For the trivial case of $V(\mathbf{R}) = 0$, the exact solution is produced.

Perhaps the best known examples demonstrating the second point are the half-filled positive- U Hubbard models and negative- U Hubbard models, two classes of models that do not have a sign problem. To illustrate the first two characteristics of the CPMC method, we consider the following half-filled positive- U Hubbard model

$$H = -t \sum_{\sigma=\uparrow,\downarrow} \left(c_{1,\sigma}^\dagger c_{2,\sigma} + c_{2,\sigma}^\dagger c_{1,\sigma} \right) + U \sum_{i=1}^2 n_{i\uparrow} n_{i\downarrow}, \quad (17)$$

which is also a simple model for a Heitler-London molecule. The two-particle ground state is given by

$$|\Psi_0\rangle = \frac{1}{\sqrt{2\tilde{t}^2 + (U - E_0)^2}} \left[\tilde{t} \left(c_{1\uparrow}^\dagger c_{1\downarrow}^\dagger + c_{2\uparrow}^\dagger c_{2\downarrow}^\dagger \right) + \frac{U - E_0}{\sqrt{2}} \left(c_{1\uparrow}^\dagger c_{2\downarrow}^\dagger + c_{2\uparrow}^\dagger c_{1\downarrow}^\dagger \right) \right] |0\rangle, \quad (18)$$

where $\tilde{t} = \sqrt{2}t$, and the ground-state energy is $E_0 = U/2 - \sqrt{(U/2)^2 + 2\tilde{t}^2}$. This state cannot be represented by a single Slater determinant, unless $U = 0$. (See Eq. 1.)

Since we want to study the nodal structure of different states, we need to parameterize the differentiable manifold of Slater determinants of two particles. We choose coordinates such that a generic point in the manifold (θ_1, θ_2) corresponds to the normalized Slater determinant

$$|\phi\rangle = \left(\cos \theta_1 c_{1\uparrow}^\dagger + \sin \theta_1 c_{2\uparrow}^\dagger \right) \left(\cos \theta_2 c_{1\downarrow}^\dagger + \sin \theta_2 c_{2\downarrow}^\dagger \right) |0\rangle. \quad (19)$$

Alternatively, from Eq. 1, we can represent this state by the product of two 2×1 matrices, i.e., $\Phi = \Phi_\uparrow \Phi_\downarrow$ where

$$\Phi_\uparrow = \begin{pmatrix} \cos \theta_1 \\ \sin \theta_1 \end{pmatrix} \quad (20)$$

and

$$\Phi_\downarrow = \begin{pmatrix} \cos \theta_2 \\ \sin \theta_2 \end{pmatrix} \quad (21)$$

Then,

$$\langle \phi | \Psi_0 \rangle = \frac{1}{\sqrt{2\tilde{t}^2 + (U - E_0)^2}} \left[\tilde{t} \cos(\theta_1 - \theta_2) + \frac{U - E_0}{\sqrt{2}} \sin(\theta_1 + \theta_2) \right]. \quad (22)$$

In Fig. 1 we display contour plots of this function for different values of U . Clearly the nodal surfaces of $\langle\phi|\Psi_0\rangle$ are different for the various values of U . Nevertheless, in the absence of importance sampling, one can prove analytically that for any U , $\langle\phi|\Psi_T\rangle = \langle\phi|\Psi_0(U=0)\rangle$ remains positive during the whole imaginary-time evolution; that is, the nodal constraint is never invoked, and therefore, the exact solution is obtained after a large- τ projection with the result that the nodal surfaces of $\langle\phi|\Psi_c\rangle$ and $\langle\phi|\Psi_0\rangle$ are the same but different from $\langle\phi|\Psi_T\rangle$.

III. MIXED ESTIMATOR OF THE ENERGY

Independent of a quantum Monte Carlo process, when is the mixed estimator for the energy (Eq. 12) an upper bound for the ground-state energy or even the exact value? Three cases are apparent:

1. If $|\Psi_T\rangle \equiv |\Psi_c\rangle$, then $E_m \geq E_0$.
2. If $|\Psi_T\rangle \equiv |\Psi_0\rangle$, or $|\Psi_c\rangle \equiv |\Psi_0\rangle$, then $E_m = E_0$.
3. If $|\Psi_c\rangle = U^{2n}|\Psi_T\rangle$, where n is an integer, U is a Hermitian operator, and $[H, U] = 0$, then $E_m \geq E_0$.

Case 1 is simply the Rayleigh-Ritz variational principle. Case 2 is perhaps the most important feature of the mixed estimator: a good approximation to the ground-state wave function will produce a good approximation to the ground-state energy. Case 3 is what happens in quantum Monte Carlo simulations: in principle, with $U = \exp[-\Delta\tau H]$, an upper bound on the energy is automatically produced. In the simulations, $U^{2n} \rightarrow U_{2n} \cdots U_2 U_1$ where $U_i = \exp[-\Delta\tau H_i]$ with H_i representing an effective Hamiltonian satisfying $[H, U_i] \neq 0$, so in general E_m is not a rigorous bound. But since $[H, U_i] \approx 0$, E_m is in general expected to be a good estimate and a bound. Clearly to the extent that the constrained-path method in principle can produce the exact state vector, the mixed estimate of energy can be exact.

On general grounds we can say that if our constrained evolution defines a Markov process with a stationary distribution $|\Psi_c\rangle$, such that

$$H_{\text{eff}}|\Psi_c\rangle = E_g|\Psi_c\rangle , \quad (23)$$

and $H_{\text{eff}} = H + \delta H$, then

$$\frac{\langle\Psi_c|H|\Psi_c\rangle}{\langle\Psi_c|\Psi_c\rangle} = E_m + \delta E_m \geq E_0 , \quad (24)$$

where

$$\delta E_m = \frac{\langle\Psi_T|\delta H|\Psi_c\rangle}{\langle\Psi_T|\Psi_c\rangle} - \frac{\langle\Psi_c|\delta H|\Psi_c\rangle}{\langle\Psi_c|\Psi_c\rangle} . \quad (25)$$

It is clear that if $\delta E_m \leq 0$, E_m is an upper bound to the ground-state energy. However, in general, this is not necessarily the case.

It is interesting to mention that in the usual fixed-node approach, where the state space manifold is the coordinate space, δH represents a hard-wall potential, i.e. it is infinite on the set of configurations $\{|\mathbf{R}_T\rangle\}$ defined by $\langle\mathbf{R}_T|\Psi_T\rangle = 0$. Then E_m is an upper bound to E_0 . We can see this by minimizing the following constrained functional

$$F\left[|\Psi_c\rangle, \langle\Psi_c|; \eta_{\mathbf{R}_T}, \eta_{\mathbf{R}_T}^*\right] = \langle\Psi_c|H|\Psi_c\rangle - E\langle\Psi_c|\Psi_c\rangle - \sum_{\mathbf{R}_T} \eta_{\mathbf{R}_T}^* \langle\mathbf{R}_T|\Psi_c\rangle - \sum_{\mathbf{R}_T} \eta_{\mathbf{R}_T} \langle\Psi_c|\mathbf{R}_T\rangle , \quad (26)$$

where $\langle\mathbf{R}_T|\Psi_T\rangle = \Psi_T(\mathbf{R}_T) = 0$ defines the nodal surface \mathcal{N}_T . The resulting Euler's equations are

$$H|\Psi_c\rangle = E|\Psi_c\rangle + \sum_{\mathbf{R}_T} \eta_{\mathbf{R}_T} |\mathbf{R}_T\rangle , \quad (27)$$

$$\langle\Psi_c|H = \langle\Psi_c|E + \sum_{\mathbf{R}_T} \eta_{\mathbf{R}_T}^* \langle\mathbf{R}_T| , \quad (28)$$

$$\Psi_c(\mathbf{R}_T) = 0 , \quad (29)$$

which lead to

$$E = \frac{\langle\Psi_T|H|\Psi_c\rangle}{\langle\Psi_T|\Psi_c\rangle} = \frac{\langle\Psi_c|H|\Psi_c\rangle}{\langle\Psi_c|\Psi_c\rangle} \geq E_0 . \quad (30)$$

From the first equation

$$\langle \mathbf{R} | H | \Psi_c \rangle = E \langle \mathbf{R} | \Psi_c \rangle + \sum_{\mathbf{R}_T} \eta_{\mathbf{R}_T} \langle \mathbf{R} | \mathbf{R}_T \rangle , \quad (31)$$

$$\sum_{\mathbf{R}'} \langle \mathbf{R} | H | \mathbf{R}' \rangle \langle \mathbf{R}' | \Psi_c \rangle = E \Psi_c(\mathbf{R}) + \sum_{\mathbf{R}_T} \eta_{\mathbf{R}_T} \delta_{\mathbf{R}\mathbf{R}_T} , \quad (32)$$

$$H(\mathbf{R}) \Psi_c(\mathbf{R}) = E \Psi_c(\mathbf{R}) + \sum_{\mathbf{R}_T} \eta_{\mathbf{R}_T} \delta_{\mathbf{R}\mathbf{R}_T} . \quad (33)$$

Solving the constrained (fixed-node) problem is equivalent to solving $H(\mathbf{R}) \Psi_c(\mathbf{R}) = E \Psi_c(\mathbf{R})$ within the region where $\Psi_T(\mathbf{R})$ has a definite sign, with the boundary condition $\Psi_c(\mathbf{R}_T) = 0$. In this way $\Psi_c(\mathbf{R})$ is a continuous function of \mathbf{R} with discontinuous derivative at $\mathbf{R} = \mathbf{R}_T$.

If we try to minimize a similar functional, but we use the representation of Slater determinants $|\phi\rangle$, then an extremely non-local term, which is not easily handled, appears in the resulting Euler equation

$$\sum_{\phi'} \langle \phi | H | \phi' \rangle \Psi_c[\phi'] = E \Psi_c[\phi'] + \sum_{\phi_T} \eta_{\phi_T} \langle \phi | \phi_T \rangle , \quad (34)$$

with $\Psi_T[\phi_T] = \langle \phi_T | \Psi_T \rangle = 0$ but in general $\langle \phi | \phi_T \rangle \neq \delta_{\phi\phi_T}$. As before, one can easily prove that $E_m \geq E_0$. In other words, if we had used the exact equivalent of the fixed-node constraint, we would have gotten a variational upper bound using E_m . It is important to stress that the constrained-path condition is a kind of global constraint as opposed to the local one that represents the fixed-node constraint in that the constrained-path condition does not impose on $\langle \phi | \Psi_c \rangle$ the same nodal hypersurface as $\langle \phi | \Psi_T \rangle$. In fact, we have numerical examples where $\langle \phi | \Psi_T \rangle$ does not define the exact nodal structure, nevertheless we get the exact ground-state energy for H , i.e. $|\Psi_c\rangle = |\Psi_0\rangle$. (See, for instance, the example shown at the end of Section II.)

IV. ENERGY ESTIMATORS BOUNDING THE GROUND-STATE ENERGY

A. Energy Bounds

It is possible to construct a variety of other estimators that produce upper bounds to the ground-state energy. In the following we assume we have a state $|\Psi_c\rangle$ that is an eigenstate of the constrained propagator:

$$|\Psi_c\rangle = \lim_{\tau \rightarrow \infty} e^{-\overleftarrow{\tau}H} |\Psi_T\rangle \quad (35)$$

with eigenvalue $\exp[-\tau E_g]$

$$e^{-\overleftarrow{\Delta\tau}H} |\Psi_c\rangle = e^{-\Delta\tau E_g} |\Psi_c\rangle . \quad (36)$$

The arrow indicates the direction of propagation with the constraint applied to the wave function. Only those auxiliary fields that retain a positive overlap with the trial function are retained in the sampling. The CPMC paths are not reversible in the standard sense, and hence the “time arrow” of the path is significant. In contrast, we denote the original unconstrained propagator as $\exp[-\tau H]$, and since H is Hermitian, the full propagation is reversible, at least when averaged over paths. The effect of the constraint is simply given by the difference between $\exp[-\overleftarrow{\tau}H]$ and $\exp[-\tau H]$.

The standard variational upper bound is given by

$$E_v = \frac{\langle \Psi_c | H | \Psi_c \rangle}{\langle \Psi_c | \Psi_c \rangle} \geq E_0 , \quad (37)$$

where the function $\langle \Psi_c |$ is the dual state of $|\Psi_c\rangle$; that is, the constraint is applied in the opposite τ direction. It is possible to calculate E_v directly, for example, by propagating two populations of random walkers. These two populations can be used as independent samples of $\langle \Psi_c |$ and of $|\Psi_c\rangle$. Since these walkers should be independently evaluated (at least prior to the introduction of importance sampling), we label them as $\langle \Psi_{lc} |$ and $|\Psi_{rc}\rangle$. The importance function will presumably have to be a function of all the relevant overlaps,

$$I = I(|\langle \Psi_{lc} | \Psi_{rc} \rangle|, \langle \Psi_T | \Psi_{rc} \rangle, \langle \Psi_{lc} | \Psi_T \rangle) . \quad (38)$$

The overlap of the left and right wave functions may be negative, so we have to assume the importance function is only a function of the magnitude of that overlap. In the absence of importance sampling, the denominator in Eq. 37 is the sum of the overlap between these two wave functions. Hence this term should be large in the importance function.

One can also evaluate the energy difference $E_d \equiv E_v - E_g$, given by:

$$\begin{aligned} e^{-\Delta\tau E_g} - e^{-\Delta\tau E_v} &\approx \Delta\tau E_d \\ &= \frac{\langle \Psi_c | e^{-\Delta\tau H} - e^{-\Delta\tau H} | \Psi_c \rangle}{\langle \Psi_c | \Psi_c \rangle}. \end{aligned} \quad (39)$$

The numerator in this expression is the result of the constraint: it is simply the overlap of $\langle \Psi_c |$ with the state $|\Psi_d\rangle$ representing the difference between the full and constrained propagation:

$$|\Psi_d\rangle = \left[e^{-\Delta\tau H} - e^{-\Delta\tau H} \right] |\Psi_c\rangle. \quad (40)$$

This difference is simply the set of the configurations discarded via the constraint. E_d is zero if these discarded configurations are, on average, orthogonal to $|\Psi_c\rangle$. In the fixed-node method the configurations thrown away are by definition orthogonal both to $|\Psi_T\rangle$ and $|\Psi_c\rangle$. Here, though, our configurations are in general orthogonal only to $|\Psi_T\rangle$, and hence the variational and mixed estimates of the energy need not be equal.

It is still true, however, that E_m and E_g are equal in the limit of zero time step. The density of configurations near the surface $\langle \Psi_T | \phi \rangle$ goes to zero rapidly so that the surface contributions to the constrained propagator do not give a finite contribution to the growth estimate of the energy.

One can evaluate E_d directly. To evaluate the energy difference we again need independent right- and left-hand wave functions $|\Psi_{rc}\rangle$ and $\langle \Psi_{lc}|$. Dividing the population into two independent halves representing the left- and right-hand states, we can evaluate the numerator by taking the overlaps of what is discarded (the difference between the full and constrained propagators acting on $|\Psi_c\rangle$) with the independent solution $\langle \Psi_c|$. The denominator is just the overlap $\langle \Psi_c | \Psi_c \rangle$ of the two solutions. For larger systems it will likely have

high statistical errors, but the numerator may be small enough that this does not matter. An explicit numerical example is presented in the next section.

There are several other ways to produce an energy difference $E_d = 0$. One possibility is to introduce a parameter in the trial state and vary it until $E_d = 0$. Another possibility is changing the constraint. For example, we could discard configurations $|\phi\rangle$ for which the normalized overlap with the trial wave function is less than or equal to some constant α :

$$\frac{\langle\Psi_T|\phi\rangle}{[\langle\Psi_T|\Psi_T\rangle\langle\phi|\phi\rangle]^{1/2}} \leq \alpha . \quad (41)$$

Varying α until the average overlap of the discarded configurations and the constrained solution $|\Psi_c\rangle$ is greater than or equal to zero produces a variational upper bound for the energy, since then $E_g \geq E_v$. In this case it is not necessary to evaluate the denominator of Eq. 39. Also, this procedure is exact for an exact constraining state, since in that case we could set $\alpha = 0$.

We note that for $\alpha \neq 0$ the mixed estimate E_m is not in general equal to the growth estimate E_g , as there is a finite surface term that contributes to the difference. In fact, the difference $E_g - E_m$ provides a measure of the error introduced by the constraint. Numerical examples are provided in the following section.

This method is general in that it produces a variational upper bound to the energy for any Hamiltonian and any constraint. The only restriction is that $|\Psi_d\rangle$ has a positive overlap with the eigenstate $\langle\Psi_c|$ of the constrained propagation. This restriction naturally implies a repulsive contribution to E_g and an increase in the value of the energy. This algorithm can be made quite general and applied to a variety of interesting situations.

B. Numerical Example

In this sub-section we consider a simple numerical example illustrating the behavior of the various energy estimators. The particular example is the 2D Hubbard model on a 4×4 lattice with 5 up spin and 5 down spin electrons. The exact ground-state energy of this small

system was obtained by direct diagonalization. For the intermediate coupling of $U = 8t$ and $t = 1$, the energy is -17.51037 .¹⁴

We used the free-particle wave functions for both the constraint and the importance function in a series of CPMC calculations. As a variational wave function, the free-particle wave functions are quite inaccurate, yielding an energy of -11.50 . We also used population sizes of 1000 to 2500 configurations, divided into two halves for independent left- and right-hand wave functions. Averages were computed over 30-100 blocks with a propagation time (number of steps times $\Delta\tau$) of 2 to 10 per block. We verified that we have reached the equilibrium state before computing averages and that the blocks were large enough to avoid difficulties with autocorrelations among individual energy estimates. All calculations were performed on single workstations, though extensions to large systems would require a parallel implementation.

The various energy estimators are plotted as a function of the size of the time step $\Delta\tau$ in Fig. 2. The exact ground-state energy is shown as a circle at the extrapolated $\Delta\tau = 0$ limit. The two dashed curves illustrate the growth and mixed estimates E_g and E_m . E_g is simply obtained from the change in overlap with iteration

$$e^{-\Delta\tau E_g} = \frac{\langle \Psi_T | \Psi_c(\tau + \Delta\tau) \rangle}{\langle \Psi_T | \Psi_c(\tau) \rangle}, \quad (42)$$

while E_m is obtained by direct evaluation of Eq. 12. Since the propagator is approximate, these two estimates coincide only in the limit of small $\Delta\tau$.

As apparent from the figure, these two estimates lie slightly below the exact energy. The value of E_g , extrapolated to $\Delta\tau = 0$, is $-17.517(2)$. During the course of this calculation, we also evaluated E_d . In this case, E_d is small and positive, and adding this difference to E_g should produce a variational upper bound to the ground-state energy. Extrapolating to $\Delta\tau = 0$, we find $E_d = 0.010(1)$, and hence $E_v = -17.506(2)$. The accuracy of the variational bound is quite surprising: the exact energy is recovered with an accuracy of two parts in 10^4 , or better than 99.9% of the difference between the exact and trial state energies.

We also plotted in Fig. 2 the result of a direct calculation of E_v . Since we have inde-

pendent calculations of the left and right-hand states, it is possible to combine these into a direct calculation of the variational energy E_v . In contrast to the other estimators, this calculation should yield a variational upper bound independent of the time step $\Delta\tau$. We find this to be true, but with a somewhat larger statistical error than the other estimators. There also appears to be some residual statistical bias resulting from the finite population size. This estimator may be more difficult to compute reliably for larger system sizes.

The statistical errors for E_d also increase rapidly with system size. Primarily this is a result of a large statistical error in the denominator (Eq. 39). Particularly for our simple choices of trial states, the overlaps of the configurations representing the left- and right-hand population can vary dramatically. The alternative method of altering the constraint slightly (Eq. 41) should produce a more favorable scaling with system size, though it remains to be demonstrated that this is practical for very large simulations.

For the 4×4 case, we explicitly changed the constraint by introducing a finite value of α . We could achieve a variational upper bound by setting $\alpha = 0.0005$; for $\alpha = 0.0003$ we could explicitly see that the sign of the overlap $\langle \Psi_c | \Psi_d \rangle$ could lead to a violation of the upper bound. For $\alpha = 0.0005$ and a time step of 0.005, we obtain a mixed estimate $E_m = -17.518(3)$ and a growth estimate $E_g = -17.505(3)$. Recall that only E_g provides an upper bound in the limit of zero time step. However, the small difference $E_m - E_g$ indicates the accuracy of the solution. Extrapolating to zero time step yields $E_g = -17.510(10)$.

We also considered a 6×6 lattice with 13 spin up and 13 spin down electrons, again for $U=8$. We are unaware of any exact or QMC calculations for this system size at this filling. These larger system size results are meant to serve as guides for future use rather than exhaustive calculations. They were obtained on single-cpu workstation over the course of a few days.

For the 6×6 system the constant α must be decreased significantly. This is rather natural as one would expect it to scale roughly with a small power of the number of single-particle orbitals. Again we use approximately 1000 configurations averaged over 30-100 individual blocks with a total propagation time of 2-4 per block. Here it is not clear if the original

choice of $\alpha = 0$ provides a variational upper bound, estimates of E_d bracket zero within the statistical errors of the calculation. For $\alpha = 0$ we obtain $E_m = E_g = -36.05(05)$.

Increasing the constant α to 10^{-6} provides a variational upper bound. In this case we obtained $E_m = -35.75(05)$ and $E_g = -34.55(10)$ for a time step of $\Delta\tau = 0.005$. Extrapolating to $\Delta\tau = 0$ yields $E_m = -35.80(05)$ and $E_g = -35.25(20)$. It is possible that this bound could be further improved by using a somewhat smaller value of α . Again, the few per cent difference between E_g and E_m indicates the accuracy of the calculation.

V. CONCLUDING REMARKS

We presented several differences between the constrained-path and fixed-node Monte Carlo methods, some major and some minor. The most significant consequence of these differences is the mixed estimator in the CPMC method not being an upper bound to the exact energy as it is in the fixed-node method. Alternate ways of producing an upper bound have been introduced.

While not an upper bound, the mixed estimator in the CPMC method was argued to be very near the exact answer. Experience shows it is almost always above the exact answer, and in cases where the CPMC results have been compared to fixed-node results, the CPMC mixed estimates of the energy always lie closer to the exact answer than the upper bound produced by the fixed-node method.¹⁵ Presumably this accuracy is a consequence of the quality of the estimates of the wave function. As a rule of thumb, we find that the fewer nodal crossings the more accurate is the prediction of the energy. This observation is supported by the method discussed in Section IV to correct the mixed estimate so it produces an upper bound. This method depends on computing a contribution from those walkers thrown away; if none are thrown away (after the sampling is from the limiting distribution), then the CPMC method in fact becomes exact.

There are several other differences between the methods worth mentioning. In one continuous spatial dimension, coincident planes ($x_i = x_j$ for all i and j corresponding to the

same spin species) exhaust the nodal surface set for local potentials V ; therefore, in the fixed-node method one can get the exact ground-state energy by using any nodal surface with this property. The free-fermion wave function suffices. For general lattice fermion problems, even in one spatial dimension, the situation is more complicated: there are extra nodal surfaces which are not coincident planes. For certain classes of Hubbard-like models the latter exhaust the whole nodal set; therefore it is possible to avoid the sign problem and get the exact solution.¹⁶ On the other hand, the lattice version of the fixed-node method¹¹ always provides a variational upper bound to the exact ground-state energy regardless of the dimensionality, unless the constraining state is the exact ground-state wave function. We have been unable to develop a similar understanding for the constrained-path method where in one dimension we observe an absence of nodal crossings and the mixed estimate of the energy agreeing with exact results to statistical accuracy.¹⁷ We comment that care must be taken in using nodal crossing rule of thumb. The accuracy of the Trotter approximation is controlled by the size of $\Delta\tau$. If $\Delta\tau$ is large, the approximation is poor, and nodal crossings can be induced into a problem for which there is no sign problem. If $\Delta\tau$ is too small, the propagation through phase space is too slow. For a poor choice of importance sampling population control can sweep away walkers that should cross the surface before they actually do.

We also remark that in the CPMC method there is much less need to perform a variational optimization of $|\Psi_T\rangle$ through Jastrow or Gutzwiller factors as seems to be necessary in the fixed-node method.⁸ This optimization process does not affect the nodal surface but does reduce the energy of the starting configuration. While there is always some advantage in doing this, the results of the CPMC method display considerable robustness to the choice of the constraining wave function which is also typically used as the starting configuration. Simple choices, like free-fermion wave functions, seem to work well. Quite different choices of $|\Psi_T\rangle$ usually give satisfyingly similar results.⁸

In closing, we remark that some of our observations about the mixed estimator for the energy might be useful in constructing and assessing estimation procedures used in the

standard auxiliary-field projector quantum Monte Carlo (AFQMC) method.^{18–20} In that method, the energy or more generally some observable \mathcal{O} is typically estimated^{21,22,19} from

$$\mathcal{O}(\tau, \tau') = \frac{\langle \Psi_T | e^{-(\tau-\tau')H} \mathcal{O} e^{-\tau'H} | \Psi_T \rangle}{\langle \Psi_T | e^{-(\tau-\tau')H} e^{-\tau'H} | \Psi_T \rangle}, \quad (43)$$

and then for large τ this expression is either averaged over several values of τ' or evaluated at just $\tau' = \tau/2$. Clearly, the latter procedure may be preferable, even though the former may have lower variance, as this estimator can be rewritten as

$$\mathcal{O}(\tau, \tau') = \frac{\langle \Psi_L | \mathcal{O} | \Psi_R \rangle}{\langle \Psi_L | \Psi_R \rangle} \quad (44)$$

revealing that for $\tau' \neq \tau$ it is basically just a mixed estimator. For estimating the energy or an observable that commutes with H , the utility of this estimator depends on how close either $\langle \Psi_L |$ or $|\Psi_R\rangle$ approaches the ground state wave function. For estimation of observables that do not commute with the Hamiltonian H , its utility depends on how close both $\langle \Psi_L |$ and $|\Psi_R\rangle$ approach the ground state wave function.

VI. ACKNOWLEDGMENTS

We gratefully acknowledge illuminating discussions with Erik Koch on the variational aspects of the constrained-path method. Most of this work was supported by the Department of Energy. S.Z. is supported by the National Science Foundation under grant DMR-9734041 and the Research Corporation.

APPENDIX: ILLUSTRATIVE EXAMPLE

We now introduce an exactly solvable fermion model to illustrate and visualize several features of the constrained-path method. This model has the Hamiltonian

$$H = -t (c_1^\dagger c_2 + c_2^\dagger c_3 + c_2^\dagger c_1 + c_3^\dagger c_2) + U (n_1 n_2 + n_2 n_3) = T + V, \quad (A1)$$

and corresponds to spinless fermions coupled through a nearest neighbor repulsive interaction U on a three site lattice with open boundary conditions. In the following we will concentrate on the two-particle solutions for which the ground state is

$$|\Psi_0\rangle = \frac{1}{\sqrt{2t^2 + (U - E_0)^2}} \left[t (c_1^\dagger c_2^\dagger + c_2^\dagger c_3^\dagger) + (U - E_0) c_1^\dagger c_3^\dagger \right] |0\rangle, \quad (\text{A2})$$

and E_0 , the ground-state energy, equals $U/2 - \sqrt{(U/2)^2 + 2t^2}$.

Since we want to study explicitly the (imaginary-time) evolution of the distribution of Slater determinants which arise as a consequence of the constrained-path approach, we need to have some way of parameterizing the differentiable manifold of Slater determinants of two particles that has dimension $N(M - N) = 2(3 - 2) = 2$. We can parameterize a state in the two-particle Hilbert space \mathcal{H}_2 that belongs to the set of *normalized* Slater determinants by the 3×2 matrix

$$\Phi = \begin{pmatrix} \cos(\theta_1 - \theta_2) & 0 \\ \cos \theta_1 & \cos \theta_2 \\ \sin \theta_1 & \sin \theta_2 \end{pmatrix}. \quad (\text{A3})$$

Therefore, the two angles (θ_1, θ_2) specify a point in the manifold, and any state $|\Psi\rangle$ belonging to the Hilbert space \mathcal{H}_2 having support in that manifold can be represented by $\Psi[\theta_1, \theta_2] \equiv \langle \phi | \Psi \rangle$. In general, the usual property of a fermion wave function to be totally antisymmetric in spin-coordinate space is lost in this new representation. For instance, the ground state of our model fermion system is given by

$$\Psi_0[\theta_1, \theta_2] = \frac{1}{\sqrt{2t^2 + (U - E_0)^2}} [\cos(\theta_1 - \theta_2) (t \cos \theta_2 + (U - E_0) \sin \theta_2) + t \sin(\theta_2 - \theta_1)], \quad (\text{A4})$$

which is neither symmetric nor anti-symmetric under permutations of θ_1 and θ_2 . Contour plots of it can be found in Fig. 3 for different values of the interaction strength U . In the non-interacting case, $U = 0$, the ground state is a single Slater determinant represented by

the matrix

$$\Phi_T = \begin{pmatrix} \sqrt{\frac{3}{4}} & 0 \\ \frac{1}{2} \left(1 + \sqrt{\frac{2}{3}}\right) & \sqrt{\frac{1}{3}} \\ \frac{1}{2} \left(\sqrt{2} - \sqrt{\frac{1}{3}}\right) & \sqrt{\frac{2}{3}} \end{pmatrix}, \quad (\text{A5})$$

corresponding to the point $\theta_{1,T} = \theta_{2,T} - \pi/6$, $\theta_{2,T} = \arccos 1/\sqrt{3}$ in the manifold.

For a given value of U we would like to project out the ground state from this non-interacting state. For simplicity, we will leave out importance sampling and use a first order Trotter decomposition for the short time propagator

$$e^{-\Delta\tau H}|\phi\rangle = e^{-\Delta\tau V} e^{-\Delta\tau T}|\phi\rangle + \mathcal{O}(\Delta\tau^2), \quad (\text{A6})$$

and stochastically iterate this expression for each walker. In a matrix representation this iteration is equivalent to a product of non-commuting random matrices, i.e. $\Phi(\tau) = \mathcal{U}(\tau)\Phi_T = \prod_{i=1}^n (\exp[-\Delta\tau V] \exp[-\Delta\tau T]) \Phi_T$, where the symmetric matrix $\exp[-\Delta\tau T]$ is given by

$$e^{-\Delta\tau T} = \begin{pmatrix} \frac{u+1}{2} & \frac{v}{\sqrt{2}} & \frac{u-1}{2} \\ \frac{v}{\sqrt{2}} & u & \frac{v}{\sqrt{2}} \\ \frac{u-1}{2} & \frac{v}{\sqrt{2}} & \frac{u+1}{2} \end{pmatrix} \quad (\text{A7})$$

with $u = \cosh(\sqrt{2} t\Delta\tau)$, $v^2 = u^2 - 1$. After the use of the discrete ($U > 0$) Hubbard-Stratonovich transformation $\exp[-\Delta\tau U n_j n_{j+1}] = \frac{1}{2} \exp[-\Delta\tau U (n_j + n_{j+1})/2] \sum_{x=\pm 1} \exp[\mu x (n_j - n_{j+1})]$, the interaction part of the propagator at any imaginary-time slice i is represented by one of the 4 diagonal random matrices (each chosen with probability 1/4, i.e. $P(\mathbf{x}) = 1/4$)

$$e^{-\Delta\tau V(i)} \equiv \begin{pmatrix} \alpha_i & 0 & 0 \\ 0 & \beta_i & 0 \\ 0 & 0 & \gamma_i \end{pmatrix} = e^{-\Delta\tau U/2} \left\{ \begin{pmatrix} e^{\pm\mu} & 0 & 0 \\ 0 & e^{-\Delta\tau U/2} & 0 \\ 0 & 0 & e^{\mp\mu} \end{pmatrix}, \begin{pmatrix} e^{\pm\mu} & 0 & 0 \\ 0 & e^{-\Delta\tau U/2 \mp 2\mu} & 0 \\ 0 & 0 & e^{\pm\mu} \end{pmatrix} \right\}, \quad (\text{A8})$$

where $\cosh \mu = \exp[\Delta\tau U/2]$. Although $\mathcal{U}(\tau)$ is a random matrix, its determinant $\det \mathcal{U}(\tau) = \exp[-2\tau U]$ is not a random number.

After a short propagation (Eq. A6), each point of the Slater determinant manifold, representing the state of the system, performs a Brownian walk in θ -space. Therefore, one can consider $\theta_1(\tau)$ and $\theta_2(\tau)$ (such that $\theta_1(0) = \theta_{1,T}$, and $\theta_2(0) = \theta_{2,T}$) as a set of random variables defining a random walker in imaginary time. However, in the CPMC method, to avoid the fermion sign problem, we constrain the walker with a constraining state which here we choose it to be $|\Psi_0(U=0)\rangle$. In other words, each time Eq. A6 is iterated, we ask, Has the sign of $\det [\Phi_T^T \Phi(\tau)]$ changed? If it has, then we kill the walker.

For the present example, the determinant can be computed analytically: At any time step $n \geq 1$

$$\det [\Phi_T^T \Phi(\tau)] = \frac{u+v}{2^{n+1}} [\alpha_1 \beta_1 f_2 + \beta_1 \gamma_1 g_2 + 2\alpha_1 \gamma_1 h_2] , \quad (\text{A9})$$

where the functions f_i , g_i and h_i are most simply obtained from the backwards recursion relations

$$\begin{aligned} f_i &= \alpha_i \beta_i (u+1) f_{i+1} + \beta_i \gamma_i (u-1) g_{i+1} + 2\alpha_i \gamma_i v h_{i+1} \\ g_i &= \alpha_i \beta_i (u-1) f_{i+1} + \beta_i \gamma_i (u+1) g_{i+1} + 2\alpha_i \gamma_i v h_{i+1} \\ h_i &= \alpha_i \beta_i v f_{i+1} + \beta_i \gamma_i v g_{i+1} + 2\alpha_i \gamma_i u h_{i+1} \end{aligned} \quad (\text{A10})$$

with $f_{n+1} = g_{n+1} = h_{n+1} = 1$ being the initial conditions.

Clearly the determinant Eq. A9 is always positive, independent of the values of n , $\Delta\tau$ and U , which means that there is no sign problem. Nevertheless, this example helps to illustrate several important issues. The first is that the exact ground-state energy can be stochastically obtained (as we will show below) even if the nodal surface of $\langle \phi | \Psi_T \rangle$ is approximate. The second issue deals with the practical numerical implementation of the method. A “false” sign problem (i.e. $\det [\Phi_T^T \Phi(\tau)] < 0$) can occur as a consequence of numerical round-off errors. In fact, the use of matrix stabilization techniques is crucial to avoid such phenomenon.²¹

Figure 4 shows the energy mixed estimator E_m as a function of imaginary time. All walkers start ($\tau = 0$) at the point $(\theta_{1,T}, \theta_{2,T})$ in θ -space. That means that $E_m(\tau = 0) = U/2 - \sqrt{2}t$, and as time evolves, $E_m \rightarrow E_0$ if the constraint is not evoked. As mentioned above this is the case if matrix stabilization techniques are properly used, otherwise we observe “false” nodal crossings. A typical random walker $\theta(\tau)$ is displayed in Fig. 5. This figure clearly denotes that most of the time the walker prefers to stay near the upper right corner of the space. This behavior is evidenced in the lower panel of the same figure, where it is shown that when the walker is at the upper right corner in θ -space the overlap with the exact ground state is maximum (in fact, it is almost one).

REFERENCES

- ¹ J.B. Anderson, *J. Chem. Phys.* **63**, 1499 (1975); **65**, 4122 (1976).
- ² Shiwei Zhang, J. Carlson, and J.E. Gubernatis, *Phys. Rev. Lett.* **74**, 3652 (1995); *Phys. Rev. B* **55**, 7464 (1997).
- ³ Several reviews include: D.M. Ceperley and M.H. Kalos, in *Monte Carlo Methods in Statistical Physics*, edited by K. Binder (Springer, Berlin, 1979); K.E. Schmidt and M.H. Kalos, in *Monte Carlo Methods in Statistical Physics II*, edited by K. Binder (Springer, Berlin, 1984); K.E. Schmidt and D.M. Ceperley, in *The Monte Carlo Method in Condensed Matter Physics*, edited by K. Binder (Springer, Berlin, 1991).
- ⁴ Shiwei Zhang, J. Carlson, and J.E. Gubernatis, *Phys. Rev. Lett.* **78**, 4486 (1997).
- ⁵ M. Guerrero, J.E. Gubernatis, and Shiwei Zhang, *Phys. Rev. B* **57**, 11980 (1998).
- ⁶ J. Bonča and J.E. Gubernatis, *Phys. Rev. B* **58**, 6992 (1998).
- ⁷ J. Bonča, J.E. Gubernatis, M. Guerrero, E. Jeckelmann, and S.R. White, *cond-mat/9712018*.
- ⁸ M. Guerrero, G. Ortiz, and J.E. Gubernatis, *Phys. Rev. B*, to appear (*cond-mat/9809040*).
- ⁹ J.W. Moskowitz, K.E. Schmidt, M.A. Lee, and M.H. Kalos, *J. Chem. Phys.* **77**, 349 (1982).
- ¹⁰ P.J. Reynolds, D.M. Ceperley, B.J. Alder, and W.A. Lester, Jr., *J. Chem. Phys.* **77**, 5593 (1982).
- ¹¹ H.J.M. van Bemmelen, D.F.B. ten Haaf, W. van Saarloos, J.M.J. van Leeuwen, and G. An, *Phys. Rev. Lett.* **72**, 2442 (1994); D.F.B. ten Haaf, H.J.M. van Bemmelen, J.M.J. van Leeuwen, W. van Saarloos, and D.M. Ceperley, *Phys. Rev. B* **51**, 13039 (1995).
- ¹² J.W. Negele and H. Orland, *Quantum Many-Particle Systems* (Addison-Wesley, Redwood City, California, 1988).

- ¹³ G. Ortiz, D.M. Ceperley, and R.M. Martin, *Phys. Rev. Lett.* **71**, 2777 (1993).
- ¹⁴ Other examples were of course computed. For example, for the same system but with $U = 20t$, the exact answer is -15.452 while the CPMC result is -15.460(3). This suggests that the violation of the upper bound does not obviously get worse as U increases. On the other hand, we know the violation cannot get worse as U decreases.
- ¹⁵ For example see, D.F.B. ten Haaf and J.M.J. van Leeuwen, cond-mat/9510042; A.C. Cosentini, M. Capone, L. Guidoni, and G.B. Bachelet, cond-mat/9801299; and G.B. Bachelet and A.C. Cosentini, cond-mat/9810173.
- ¹⁶ M.A. Lee, K.A. Motakabbir, and K.E. Schmidt, *Phys. Rev. Lett.* **53**, 1191 (1984).
- ¹⁷ R.T. Clay and J.E. Gubernatis, private communication.
- ¹⁸ G. Sugiyama and S.E. Koonin, *Ann. Phys.* **168**, 1 (1986).
- ¹⁹ S. Sorella, S. Baroni, R. Car, and M. Parrinello, *Europhys. Lett.* **8**, 663 (1989); see also S. Sorella, in *Quantum Methods in Condensed Matter Physics*, edited by M. Suzuki (World Scientific, Singapore, 1993).
- ²⁰ S.R. White, D.J. Scalapino, R.L. Sugar, E.Y. Loh, J.E. Gubernatis, and R.T. Scalettar, *Phys. Rev. B* **40**, 506 (1989).
- ²¹ E.Y. Loh, Jr and J.E. Gubernatis, in *Electronic Phase Transitions*, edited by W. Hanke and Yu.V. Kopaev (Elsevier, Amsterdam, 1992).
- ²² D.R. Hamann and S.B. Fahy, *Phys. Rev. B* **41**, 11352 (1990).

FIGURES

FIG. 1. Contour plots of the two-fermion ground-state wave function $\langle\phi|\Psi_0\rangle$ for various values of the interaction strength U/t . Notice the differences among the nodal structures.

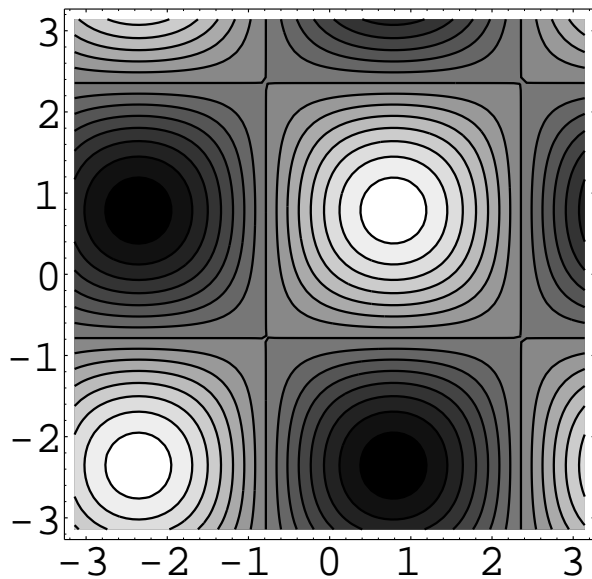
FIG. 2. Energy estimators as a function of time step for the 4×4 Hubbard model described in the text. Solid symbols indicate estimators which are variational upper bounds to the exact energy.

FIG. 3. Contour plots of the two-fermion ground-state wave function $\langle\phi|\Psi_0\rangle$ for various values of the interaction strength U/t .

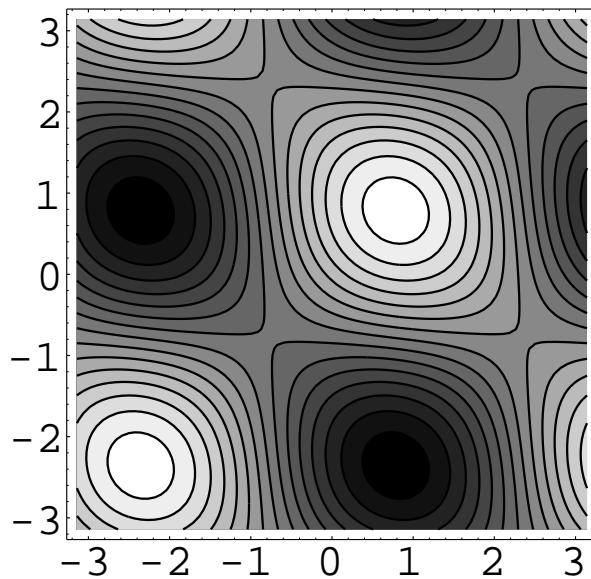
FIG. 4. Energy mixed estimator as a function of imaginary time averaged over N_w walkers. The horizontal dashed line indicates the value of the exact ground-state energy $E_0 = -0.19615t$.

FIG. 5. The upper panel shows a typical random walk in θ -space. At $\tau=0$ the walker starts at $(\theta_{1,T}, \theta_{2,T})$. The random walk never crosses the nodal surface of $\langle\phi|\Psi_T\rangle$. The lower panel displays the overlap of the walker with the exact ground state, and the distance of the walker from the origin. Notice the clear correlation between these two quantities.

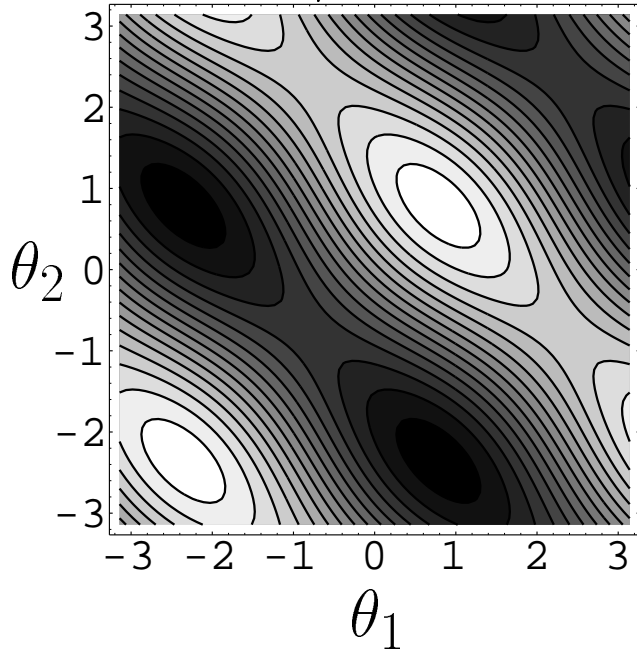
$U/t = 0$



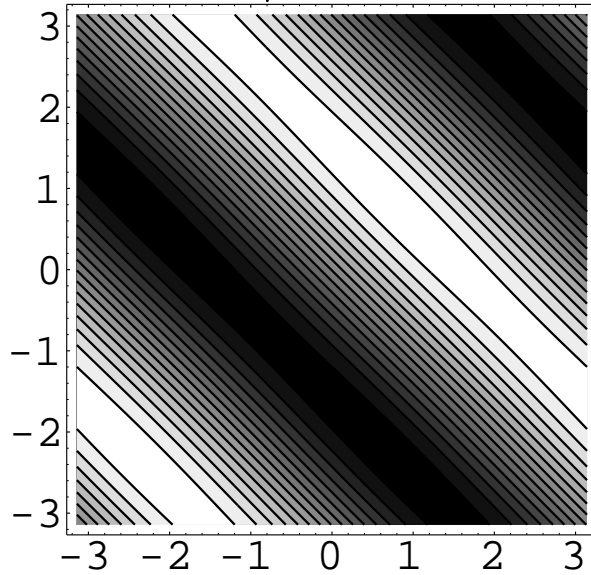
$U/t = 1$



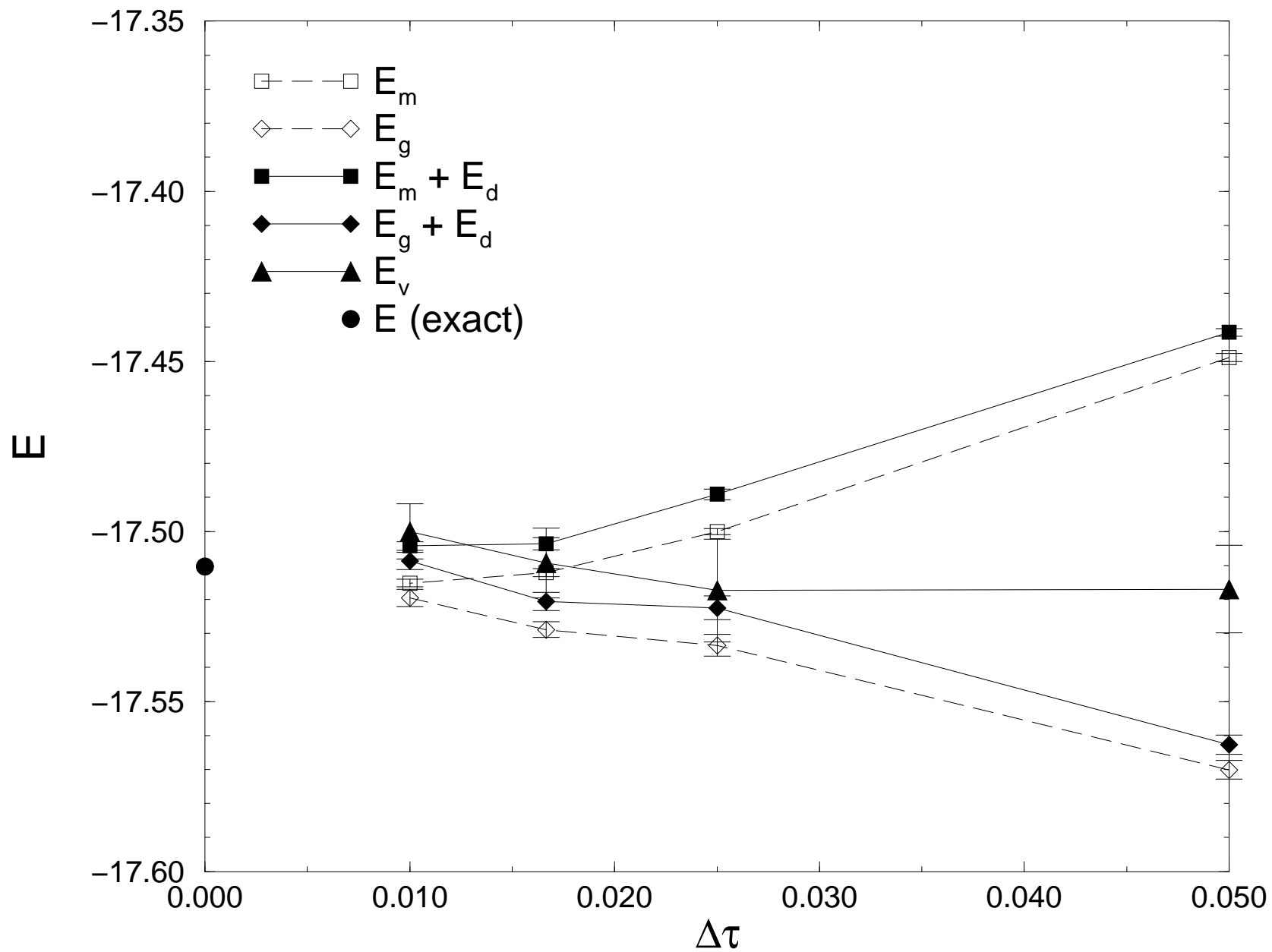
$U/t = 8$



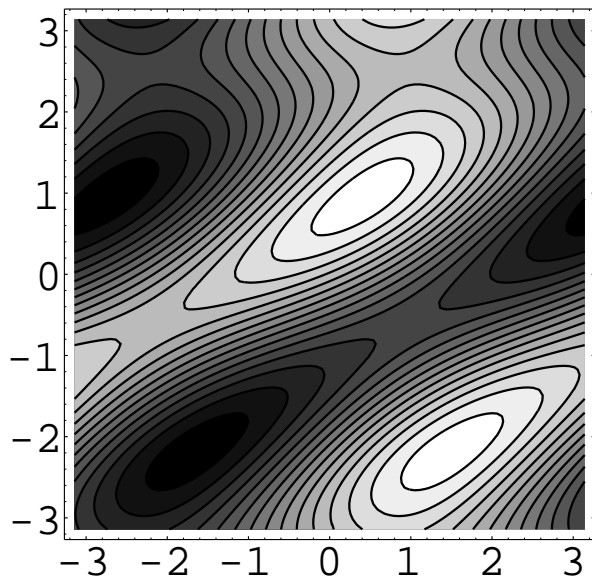
$U/t \rightarrow \infty$



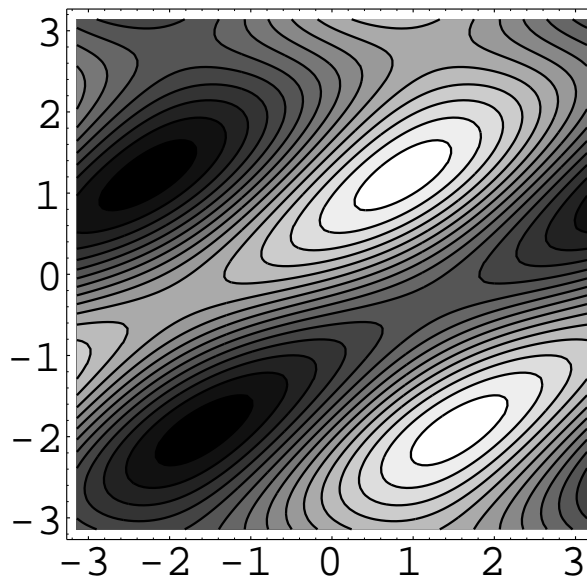
4X4 U=8 5u5d



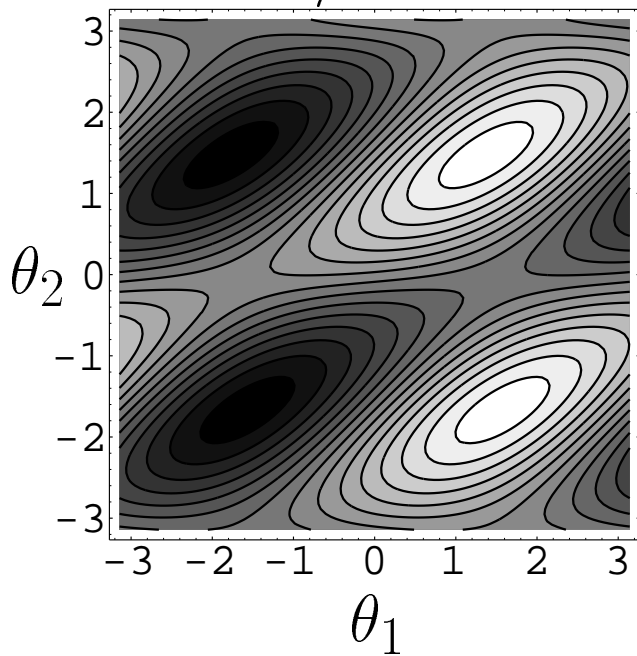
$U/t = 0$



$U/t = 2$



$U/t = 10$



$U/t \rightarrow \infty$

